Toward a Realization of Marr's Theory of Primal Sketches via Autocorrelation Wavelets: Image Representation using Multiscale Edge Information

Naoki Saito[1]

Department of Mathematics
University of California, Davis

December 1, 2005

[1] Acknowledgment: Gregory Beylkin (Colorado, Boulder), Bruno Olshausen (UC Berkeley)

Outline

Outline

Motivations

- Multiscale image analysis and Neurophysiology
  - Edge detection
  - Edge characterization
  - Shift invariance
- David Marr's conjecture: Multiscale edge information can completely represent an input image.
- Relevance of wavelets on the above issues

Outline

Introduction to Marr's Theory

- David Marr (1945–1980) proposed the following strategy/processes for visual perception
  - Raw Primal Sketch $\sim$ Edge detection, characterization $\sim$ Retina, V1
  - Full Primal Sketch $\sim$ Grouping, edge integration $\sim$ V1, V2
  - $2\frac{1}{2}$D Sketch $\sim$ Recognition of visible surfaces $\sim$ V2?, V4?
  - 3D Model Representations $\sim$ Recognition of 3D object shapes $\sim$ IT?
- Our primary focus today is a part of Raw Primal Sketch, i.e., edge detection and characterization, and how to represent an image using multiscale edge information.
- Truth is much more complicated (and interesting) due to color and motion, but we will focus on still images of intensity (grayscale) today.

Basic Neurophysiology of Visual Systems

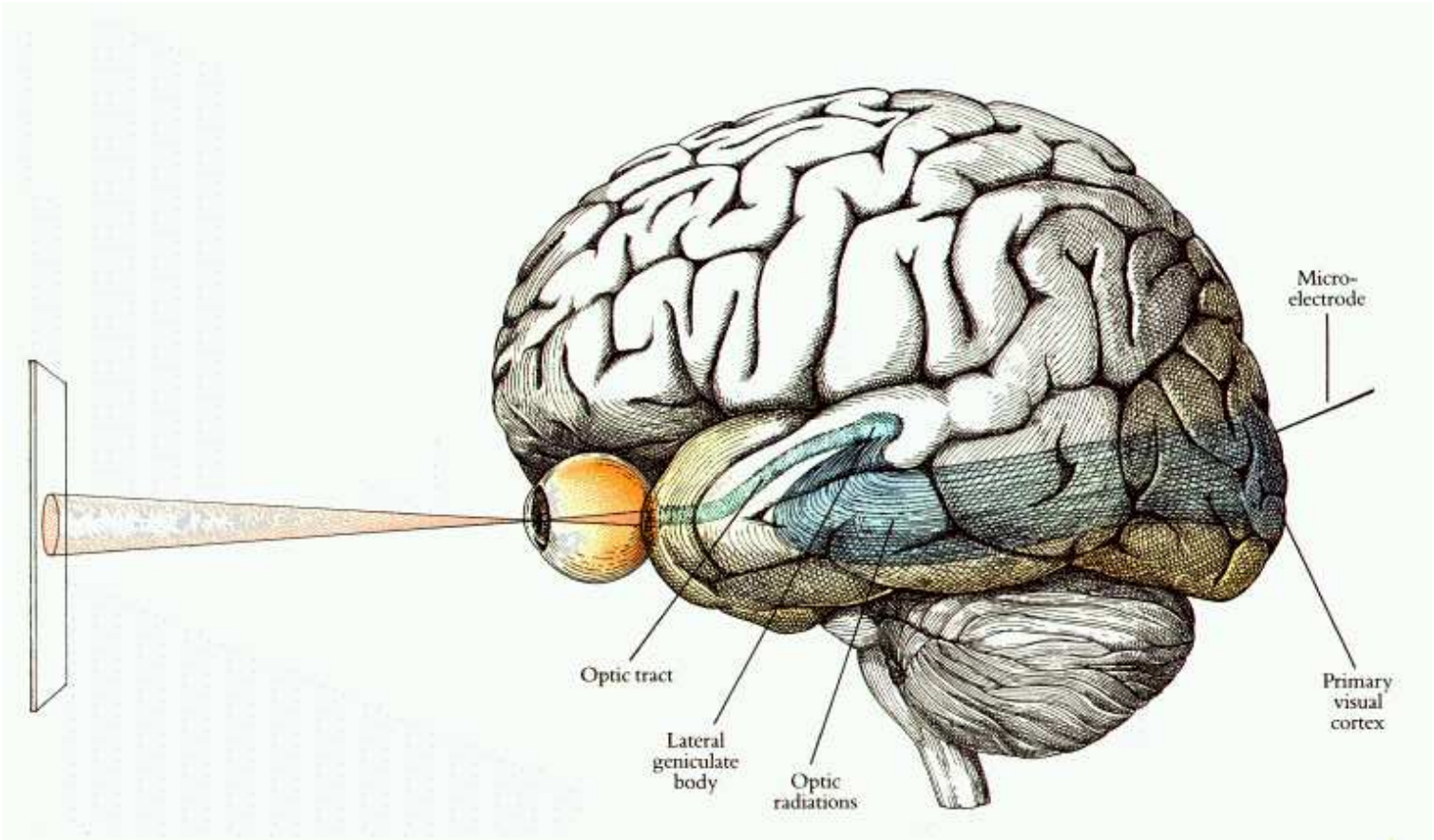

Figure: V1 area and visual passways (From D. Hubel: *Eye, Brain, and Vision*)

Basic Neurophysiology of Visual Systems . . .

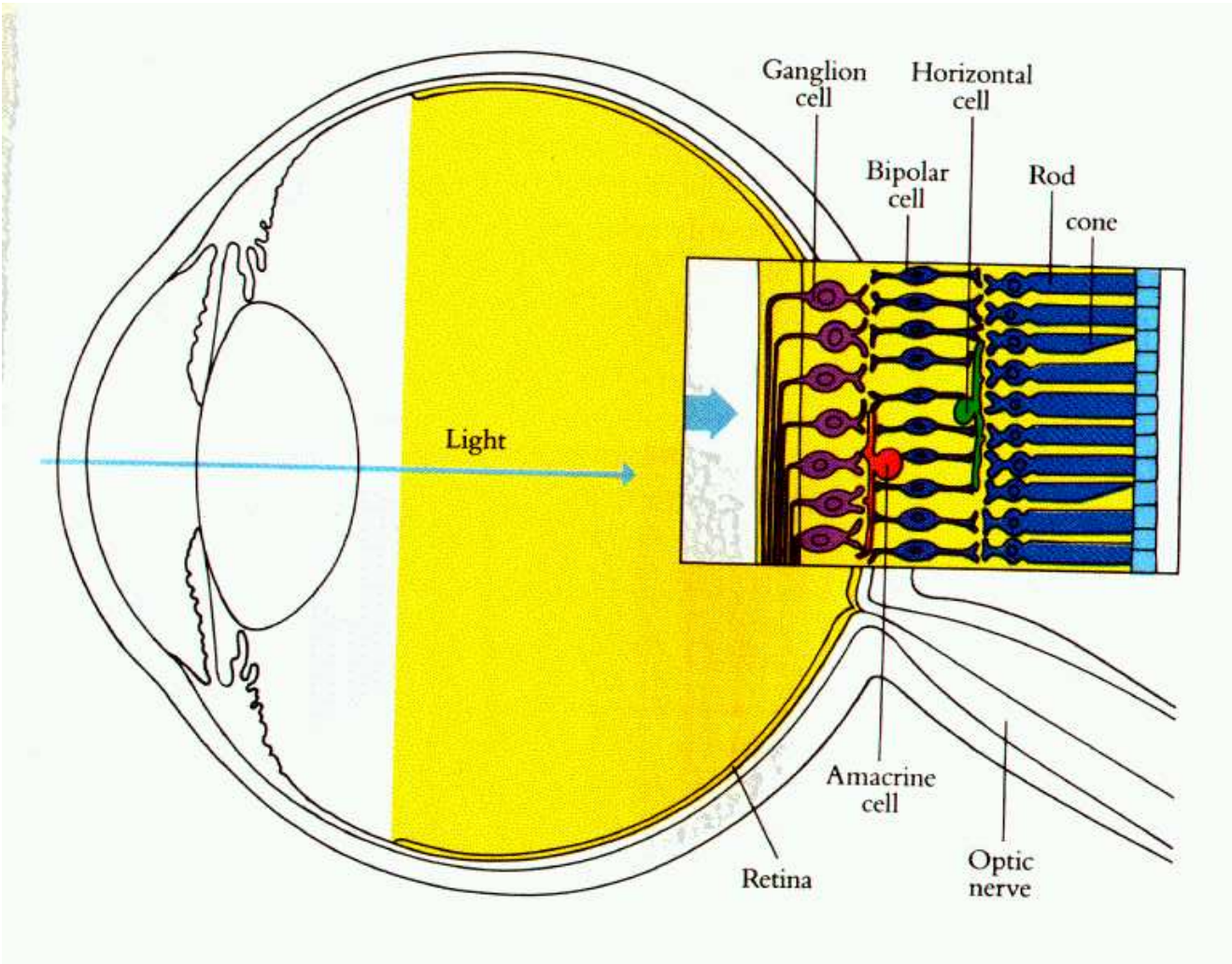

Figure: Structure of retina (From D. Hubel: *Eye, Brain, and Vision*)

Basic Neurophysiology of Visual Systems . . .

- Receptive Field of a sensory neuron $\stackrel{\Delta}{=}$ a spatial region in which the presence of a stimulus will alter the firing of that neuron.
- Spatial organization of receptive fields of retinal ganglion cells (Kuffler, 1953)
  - circularly symmetric
  - a central excitatory region
  - an inhibitory surround
- This implies that they can detect edges.

Receptive Fields

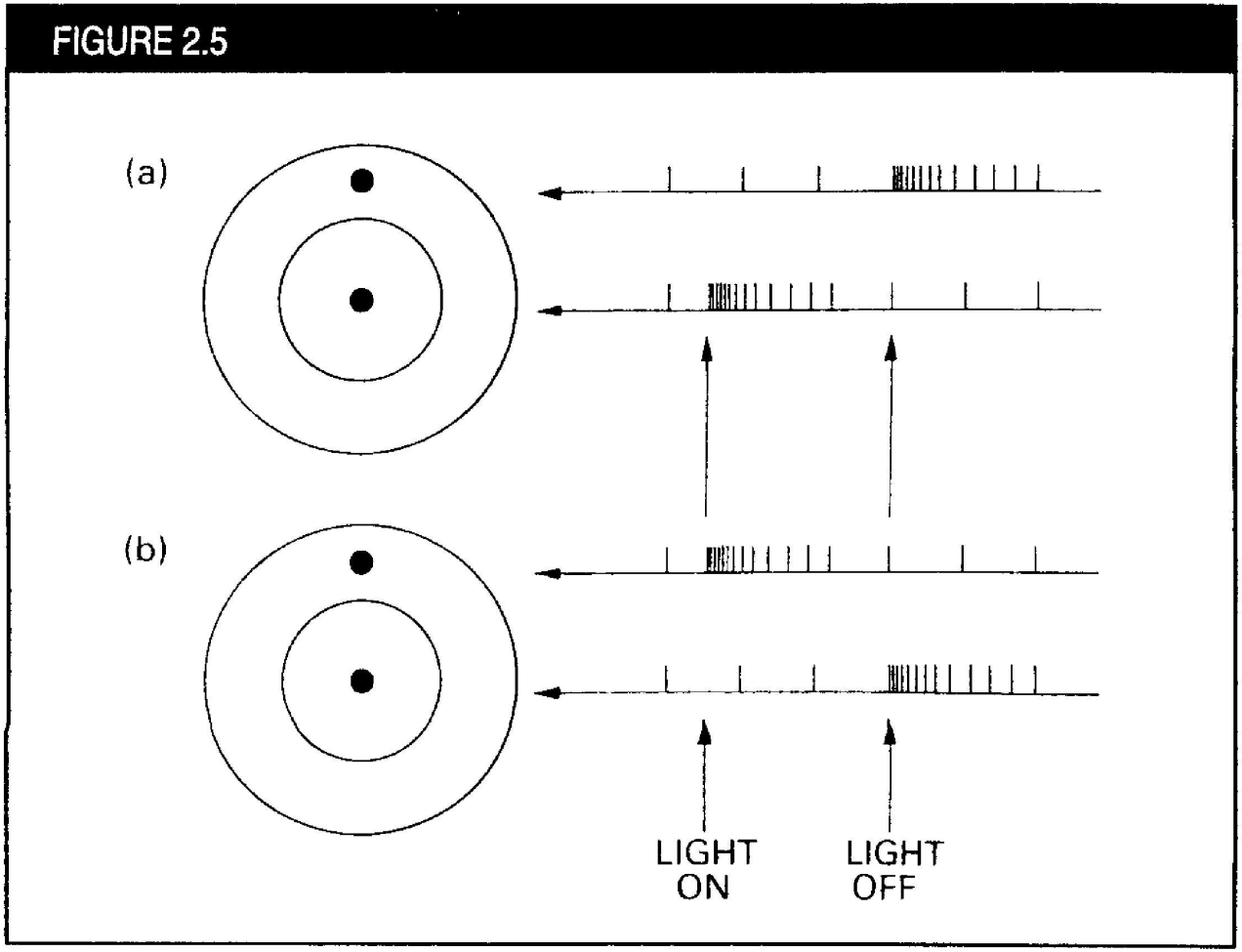

The responses of cat retinal ganglion cells to spots of light. A centre-on cell (a) responds with a burst of impulses to the onset of a spot of light *in the centre of* its field or to the offset of a spot of light in the surround area. A centre-off cell (b) responds in the opposite fashion.

Figure: Receptive field responses of ganglion cells (From V. Bruce et al.: *Visual Perception*)

Receptive Fields

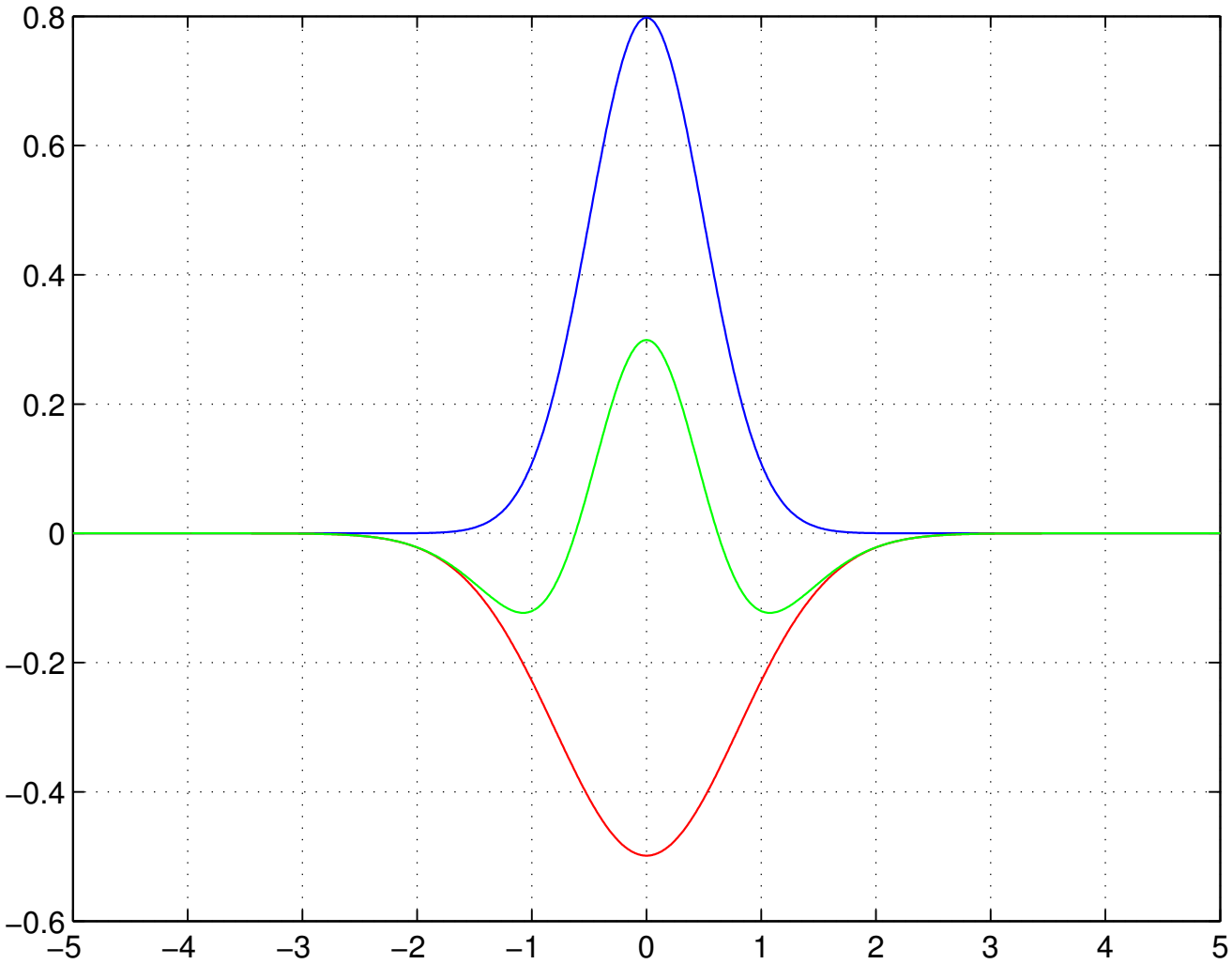

Figure: Realization of on-center off-surround receptive field (green) by a Difference of Gaussians (DOG) function (Enroth-Cugell & Robson, 1966).

The Marr-Hildreth Theory of Zero-Crossings

- Marr's idea: Multiscale edges can represent an input image
- Marr and Hildreth approximated the receptive fields as Laplacian of Gaussian (LoG), which in turn can be closely approximated by Difference of Gaussians (DOG).
- They are regularized 2nd derivative operator.
- Zero-crossings of the convolution of these filters with the input image encode the location of edges at appropriate scales.
- Slope (or gradient) at each zero-crossing encodes edge strength ($\approx$ sharpness) at appropriate scales.
- How to use the edge information to recover or represent the original image?

Edge Detection and Zero-Crossings

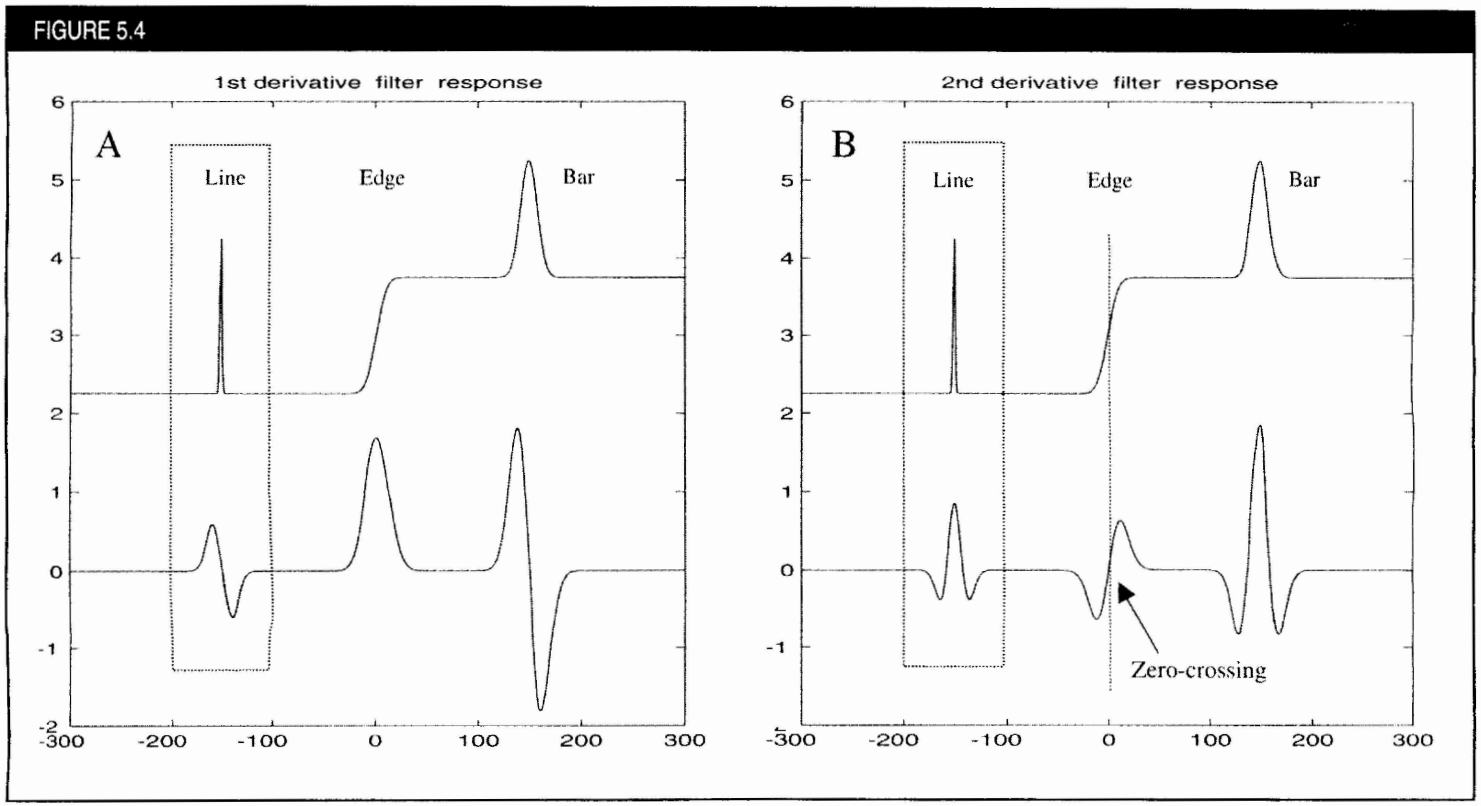

Measuring image gradients and derivatives. (A) Top trace is the stimulus luminance profile, representing a thin bright line, a blurred edge, and a blurred bar. The trace below is the response profile of a 1st derivative (gradient) filter. Note how there is a peak response (gradient maximum) at the edge location, but a peak and trough around the line and bar locations. (B) Similar layout, but the filter is a 2nd derivative operator, as used by the Marr and Hildreth (1980) and Watt and Morgan (1985) models of feature representation. Note how the zero-crossing lines up with the edge location (dotted line). The response to a thin line (left part of each panel) reveals the profile of each filter's receptive field—two-lobed (A) and three-lobed (B). These plots illustrate a key problem for early spatial vision: how is the information from spatial filters used to derive a description of the locations and characteristics of features present in the image?

Figure: Responses of 1st and 2nd derivative operators to various features (From V. Bruce et al.: *Visual Perception*)

Laplacian of Gaussian Filtering

Zero-Crossings of LoG filtered images

Zero-Crossings of LoG filtered images (Thresholded)

Wavelets in V1?

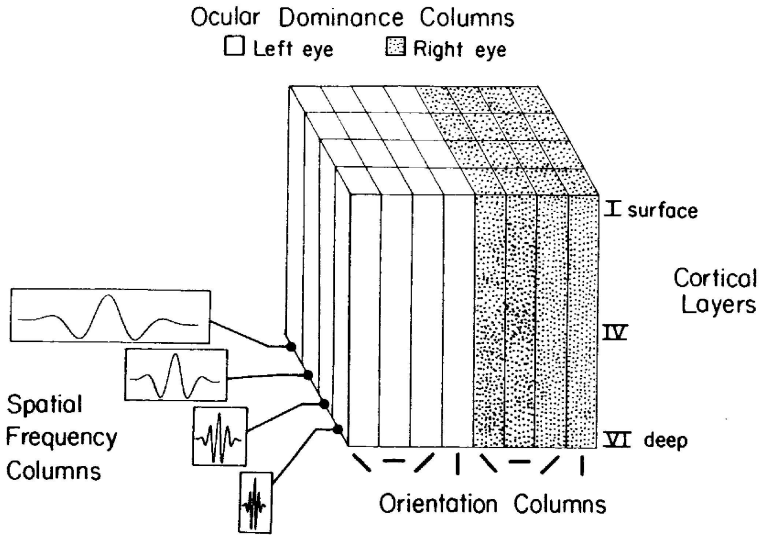

Model of Striate Module in Cats

FIG. 4.23 Schematic model of the columnar organization of cat striate cortex. Within each ocular dominance region are orthogonally arranged columns of cells tuned to different spatial frequencies and different orientations such that all spatial frequency/orientation combinations occur within each module.

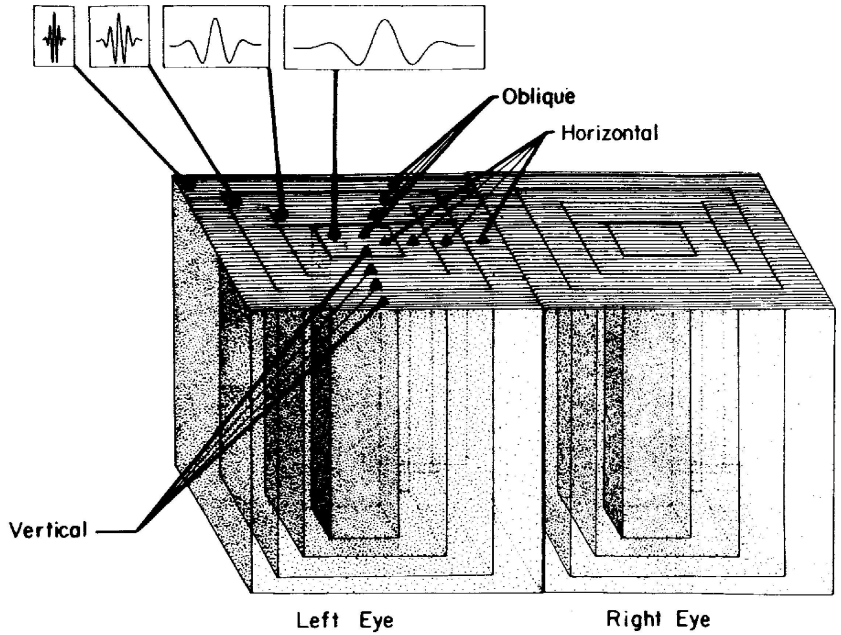

Model of Striate Module in Monkeys

FIG. 4.25 Schematic model of the columnar organization of primate striate cortex. The various two-dimensional spatial frequencies are postulated to be in a polar arrangement, with spatial frequency increasing from the center (coincident with the cyt-ox blob for that half module) out and orientation being represented at various angles.

Figure: Columnar organization of V1 cells of cats and monkeys (From: R. L. De Valois & K. K. De Valois: *Spatial Vision*)

Forming Scale and Orientation Selectivity in V1

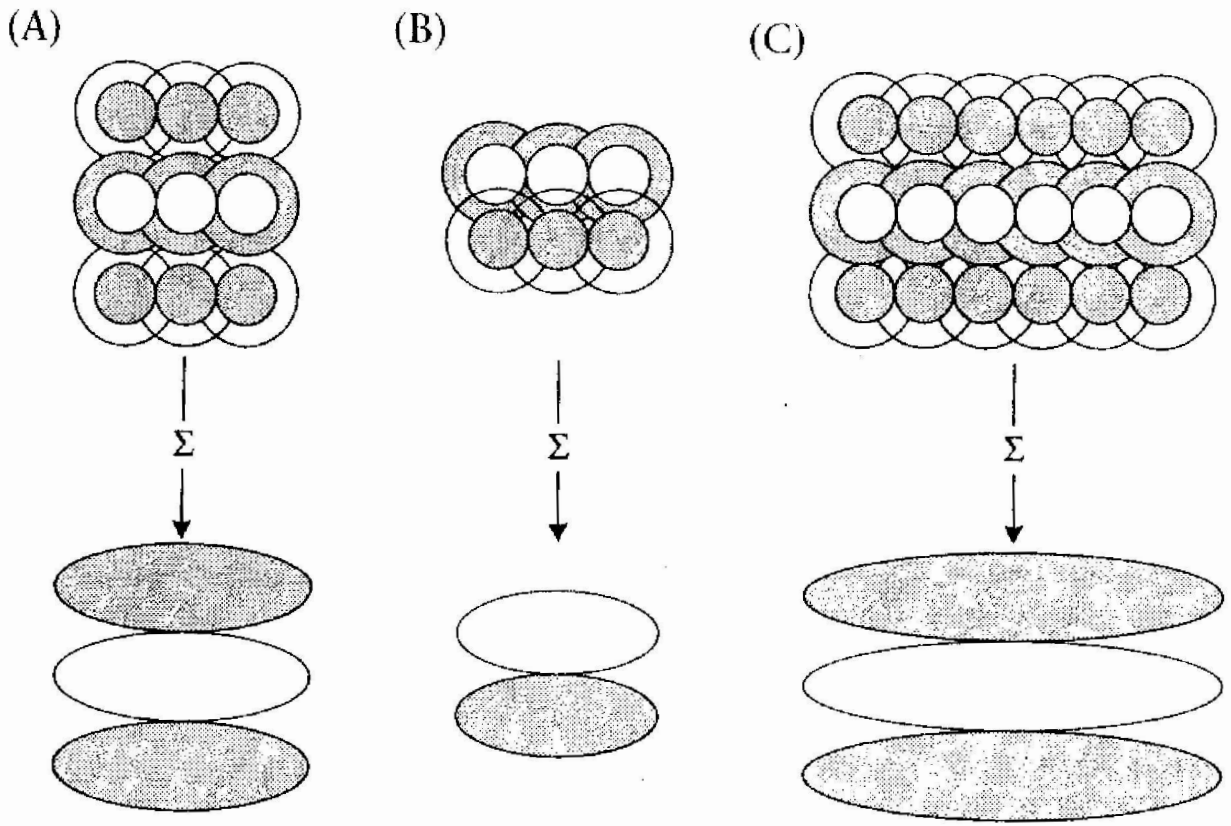

6.9 ORIENTATION-SELECTIVE RECEPTIVE FIELDS can be created by summing the responses of neurons with nonoriented, circularly symmetric receptive fields. The receptive fields of three hypothetical neurons are shown. Each hypothetical receptive field has adjacent excitatory and inhibitory regions. A comparison of (A) and (C) illustrates that the degree of orientation selectivity can vary depending on the number of neurons combined along the main axis.

Figure: Various summations of ganglion receptive fields (From: B. A. Wandell: *Foundations of Vision*)

Why Not Use Different Wavelets as a Multiscale Edge Detector?

- Multiscale LoGs in fact form a continuous wavelet transform.
- But rather slow computationally.
- Can we use faster popular discrete wavelets?
- Can we view them as multiscale edge detectors and receptive fields?
- Yes. But we need to know a little bit about the wavelet basics!
- I will concentrate on the 1D case in this talk from now on. For 2D, it's possible to do via tensor product.
- You are more than welcome to work on this area with me if you are interested. The project with my former intern has not been completed yet for 2D.

Outline

What Are Wavelets?

- An orthonormal basis of $L^2(\mathbb{R})$ generated by dilations (scalings) and translations (shifts) of a single function
- Provide an intermediate representation of signals between space domain and frequency domain (space-scale representation)
- A computationally efficient algorithm ($O(N)$) exists for expanding a discrete signal of length N into such a wavelet basis
- Useful for signal processing, numerical analysis, statistics ...

Familiar Examples

- The Haar functions

$$\psi_{\text{Haar}}(x) = \begin{cases} 1 & \text{if } 0 \le x \le \frac{1}{2} \\ -1 & \text{if } \frac{1}{2} \le x \le 1 \\ 0 & \text{otherwise.} \end{cases}$$

- The Shannon (or Littlewood-Paley) wavelets: Dilations and translations of the perfect band-pass filter

$$\psi_\infty(x) = 2\ \text{sinc}(2x) - \text{sinc}(x) = \frac{\sin 2\pi x - \sin \pi x}{\pi x}.$$

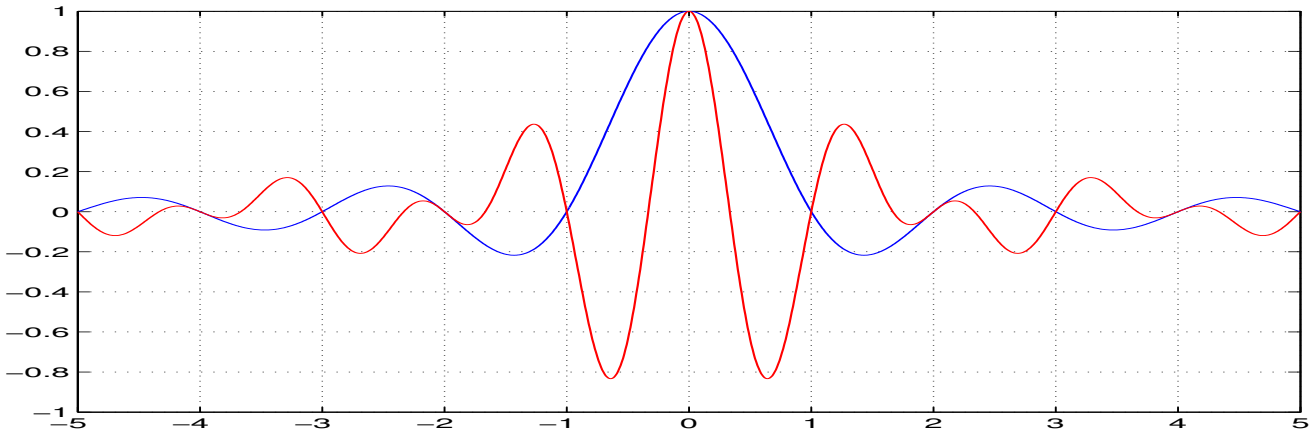

Multiresolution Analysis

- A natural framework to understand wavelets developed by S. Mallat & Y. Meyer (1986)
- Successive approximations of $L^2(\mathbb{R})$ with multiple resolutions
- $\cdots \subset \mathcal{V}_2 \subset \mathcal{V}_1 \subset \mathcal{V}_0 \subset \mathcal{V}_{-1} \subset \mathcal{V}_{-2} \subset \cdots$
- $\bigcap_{j \in \mathbf{Z}} \mathcal{V}_j = \{0\}, \quad \overline{\bigcup_{j \in \mathbf{Z}} \mathcal{V}_j} = L^2(\mathbb{R})$
- $f(x) \in \mathcal{V}_j \Longleftrightarrow f(2x) \in \mathcal{V}_{j-1}, \quad \forall j \in \mathbb{Z}$
- $f(x) \in \mathcal{V}_j \Longleftrightarrow f(x - 2^j k) \in \mathcal{V}_j, \quad \forall k \in \mathbb{Z}$
- $\exists 1\ \varphi(x) \in \mathcal{V}_0$ (scaling function or father wavelet), such that $\{\varphi_{j,k}(x)\}_{k \in \mathbb{Z}}$, where $\varphi_{j,k}(x) \stackrel{\Delta}{=} 2^{-j/2}\varphi(2^{-j}x - k)$, form an orthonormal basis of $\mathcal{V}_j$

Multiresolution Analysis . . .

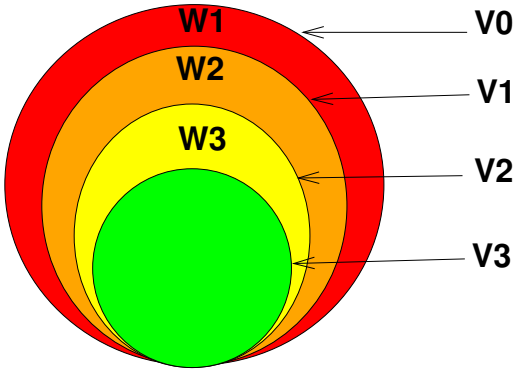

The Concept of Multiresolution Analysis

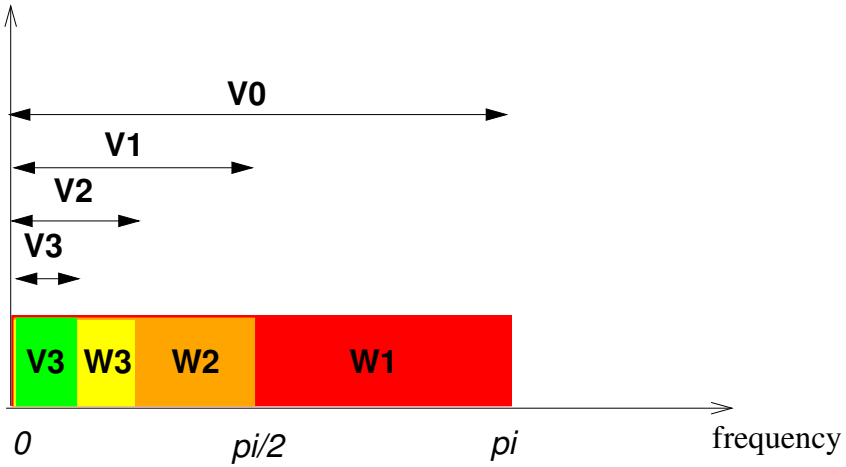

Multiresolution Analysis by Sinc Wavelets

Multiresolution Analysis . . .

- Since $\mathcal{V}_0 \subset \mathcal{V}_{-1}$, there exist coefficients $\{h_k\} \in \ell^2(\mathbb{Z})$ such that

$$\varphi(x) = \sqrt{2} \sum_k h_k \varphi(2x - k),$$

where

$$h_k = \langle \varphi, \varphi_{1,k} \rangle = \sqrt{2} \int \varphi(x)\varphi(2x - k)\, \mathrm{d}x.$$

- From the orthonormality of $\{\varphi_{0,k}\}$, the coefficients $\{h_k\}$ must satisfy

$$\sum_k h_k h_{k+2l} = \delta_{0,l}$$

Multiresolution Analysis . . .

Let us now consider the orthogonal complement $\mathcal{W}_j$ of $\mathcal{V}_j$ in $\mathcal{V}_{j-1}$.

- $V_{j-1} = \mathcal{V}_j \oplus \mathcal{W}_j$.
- $L^2(\mathbb{R}) = \bigoplus_{j\in\mathbb{Z}} \mathcal{W}_j$.
- $\exists 1\ \psi(x) \in \mathcal{W}_0$ (basic wavelet or mother wavelet), such that $\{\psi_{j,k}(x)\}_{(j,k)\in\mathbb{Z}^2}$, where $\psi_{j,k}(x) \stackrel{\Delta}{=} 2^{-j/2}\psi(2^{-j}x - k)$, form an orthonormal basis of $L^2(\mathbb{R})$.

$$\psi(x) = \sqrt{2}\sum_k g_k \varphi(2x - k), \quad g_k = (-1)^k h_{1-k}.$$

Familiar Examples

- If $h_0 = h_1 = 1/\sqrt{2}$, then

$$\begin{aligned} \varphi(x) &= \chi_{[0,1]}(x) \\ &= \chi_{[0,1]}(2x) + \chi_{[0,1]}(2x-1) \\ &= \chi_{[0,\frac{1}{2}]}(x) + \chi_{[\frac{1}{2},1]}(x). \end{aligned}$$

$$\begin{aligned} \psi(x) &= \psi_{\text{Haar}}(x) \\ &= \chi_{[0,\frac{1}{2}]}(x) - \chi_{[\frac{1}{2},1]}(x). \end{aligned}$$

- If $h_k = \text{sinc}(k/2)/\sqrt{2}$, $k \in \mathbb{Z}$, then

$$\varphi(x) = \text{sinc}(x),$$

$$\psi(x) = \psi_\infty(x) = 2\ \text{sinc}(2x) - \text{sinc}(x).$$

Multiresolution Analysis . . .

- In the Fourier domain,

$$\hat{\varphi}(\xi) = m_0(\xi/2)\hat{\varphi}(\xi/2),$$

$$\hat{\psi}(\xi) = m_1(\xi/2)\hat{\varphi}(\xi/2),$$

where

$$m_0(\xi) = \frac{1}{\sqrt{2}} \sum_k h_k \mathrm{e}^{\mathrm{i}k\xi},$$

$$m_1(\xi) = \frac{1}{\sqrt{2}} \sum_k g_k \mathrm{e}^{\mathrm{i}k\xi} = \mathrm{e}^{\mathrm{i}(\xi+\pi)} \overline{m_0(\xi+\pi)}.$$

- The filters $H = \{h_k\}$ and $G = \{g_k\}$ are called quadrature mirror filters (QMF) since they satisfy

$$|m_0(\xi)|^2 + |m_1(\xi)|^2 = 1.$$

Multiresolution Analysis . . .

- From these properties, we have

$$|\hat{\varphi}(\xi)|^2 = |\hat{\varphi}(\xi/2)|^2 + |\hat{\psi}(\xi/2)|^2,$$

$$\hat{\varphi}(\xi) = \prod_{j=1}^{\infty} m_0(\xi/2^j),$$

$$\hat{\psi}(\xi) = m_1(\xi/2) \prod_{j=2}^{\infty} m_0(\xi/2^j).$$

Compactly Supported Wavelets of Daubechies

- Once the coefficients $\{h_k\}$ are chosen, the father and mother wavelets are completely determined
- $\{h_k\}$ of finite length $\Longrightarrow$ compactly supported father and mother wavelets
- In 1987, I. Daubechies found a way to determine $\{h_k\}$ of finite length, L
- Compact support:

$$|\text{supp } \varphi| = |\text{supp } \psi| = L - 1$$

- Regularity: $\psi \in C^{\gamma(M-1)}$, $\gamma \approx 1/5$
- Vanishing moments ($L = 2M$):

$$\int x^m \psi(x)\,\mathrm{d}x = 0, \quad \text{for } m = 0, 1, \ldots, M-1$$

Problems of Orthonormal Wavelet Basis

- Provide nonredundant compact representation $\Longrightarrow$ Very useful for signal compression, in particular, piecewise smooth data.
- However, it does not provide shift invariant representation. The relation between the wavelet coefficients of the original and those of the shifted version is complicated unlike the usual Fourier coefficients.
- Except for $L = 2$ (Haar), φ and ψ are neither symmetric nor antisymmetric, thus some artifacts become visible if the input signal is severely compressed.
- First we tackle the shift-invariance problem.

Outline

Orthonormal Shell Representation

- A shift-invariant representation using the orthonormal wavelets
- Redundant but contains all orthonormal wavelet coefficients of all circular shifts of the original signal
- Computational cost is $O(N \log_2 N)$ where $N = \#$ of input samples

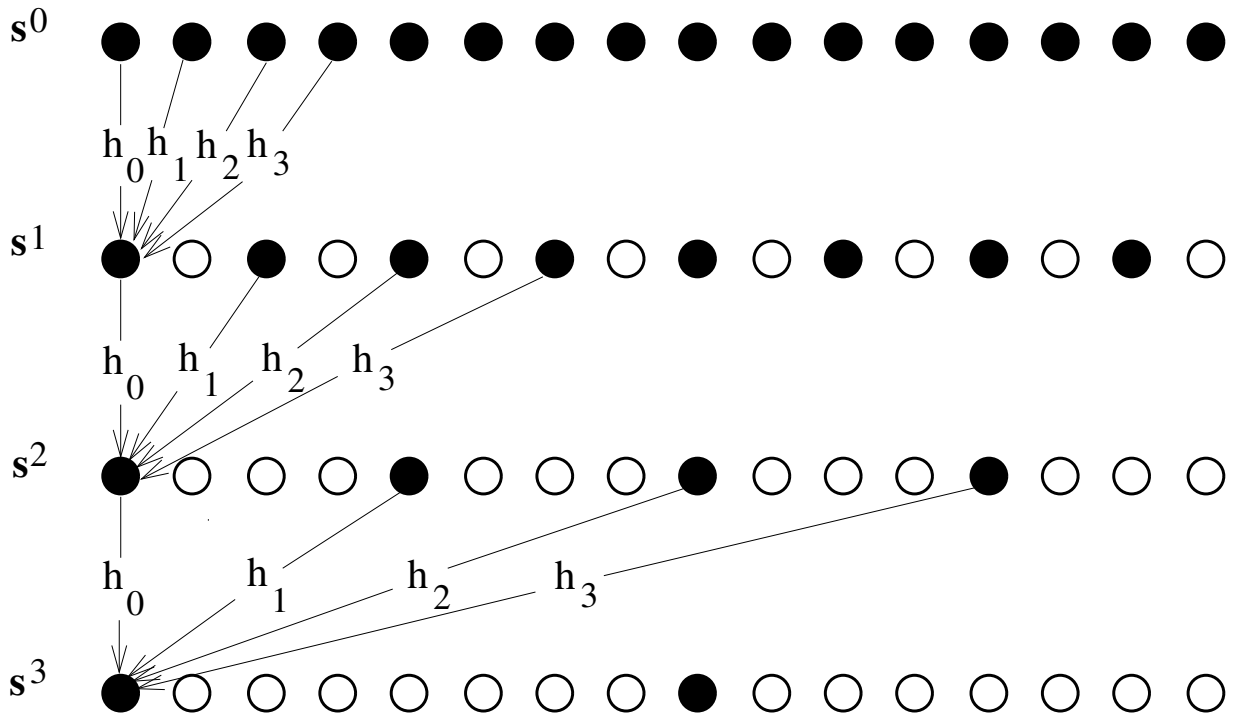

Figure: Filled circles: wavelet coefficients; Filled & open circles: orthonormal shell coefficients

Orthonormal Shell Representation . . .

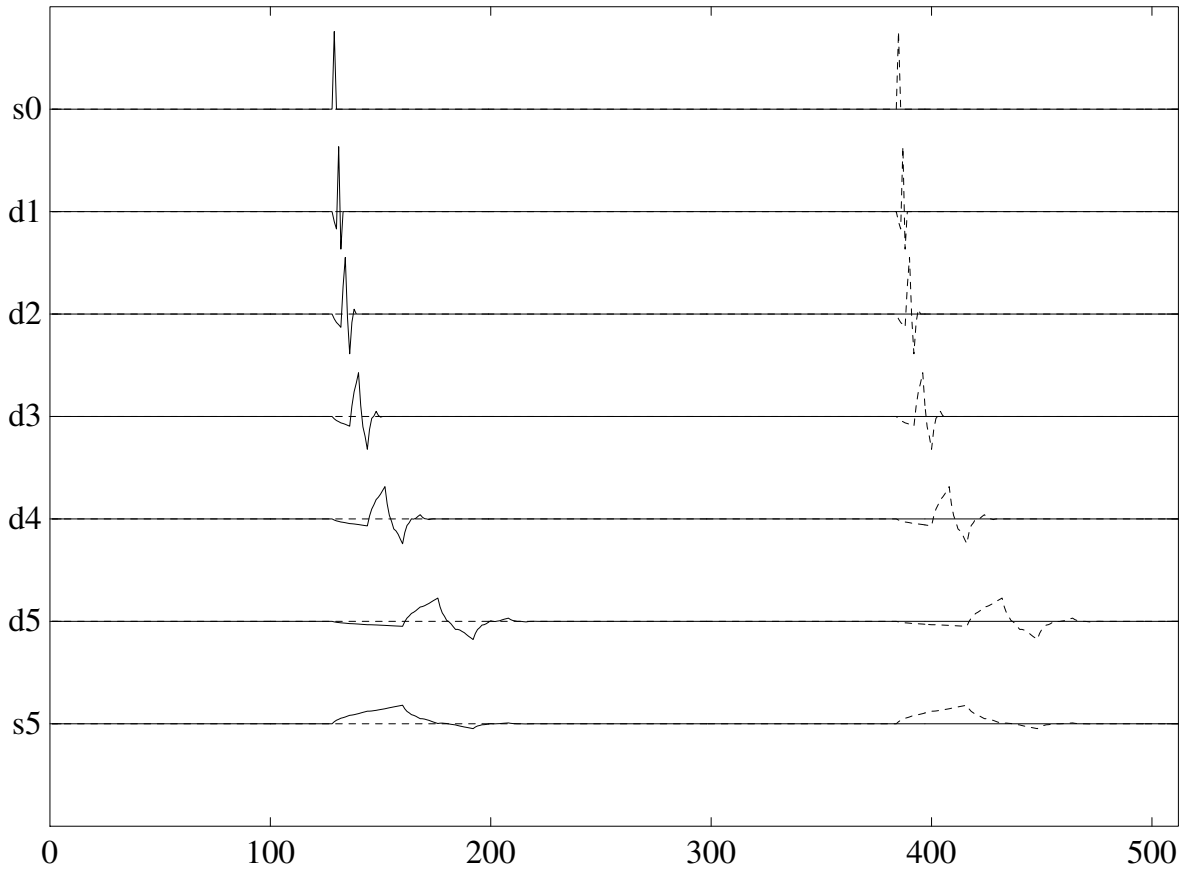

Figure: ONS representation of two spikes.

Orthonormal Shell

- An orthonormal shell is a set of functions

$$\left\{\widetilde{\psi}_{j,k}(x)\right\}_{1\le j\le J,\ 0\le k\le N-1} \quad \text{and} \quad \{\widetilde{\varphi}_{J,k}(x)\}_{0\le k\le N-1},$$

  where

$$\widetilde{\varphi}_{j,k}(x) \triangleq 2^{-j/2}\varphi(2^{-j}(x-k)), \widetilde{\psi}_{j,k}(x) \triangleq 2^{-j/2}\psi(2^{-j}(x-k))$$

- The orthonormal shell coefficients of a function $f \in \mathcal{V}_0$, $f = \sum_{k=0}^{N-1} s_k^0 \varphi_{0,k}$, are $\{d_k^j\}_{1\le j\le J,\ 0\le k\le N-1}$ and $\{s_k^J\}_{0\le k\le N-1}$, where

$$s_k^j = \int f(x)\widetilde{\varphi}_{j,k}(x)\,\mathrm{d}x, \quad d_k^j = \int f(x)\widetilde{\psi}_{j,k}(x)\,\mathrm{d}x$$

Orthonormal Shell Representation . . .

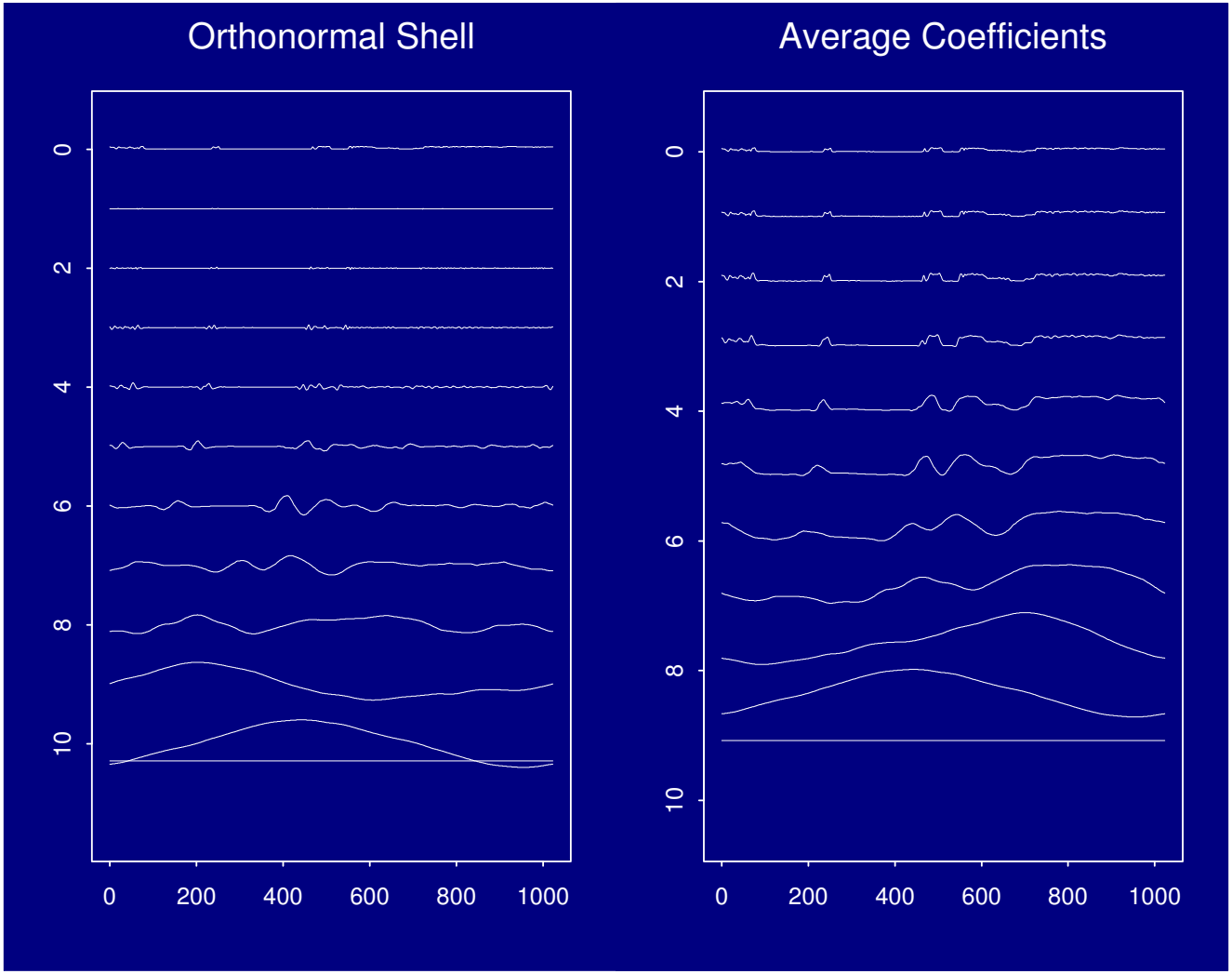

Figure: ONS representation of a real signal.

Difficulties of Orthonormal Shell

- Asymmetry of the orthonormal wavelets $\longrightarrow$ Difficulty in feature matching from scale to scale.
- Fractal-like shapes of the orthonormal wavelets $\longrightarrow$ Too many zero-crossings/extrema.

Outline

Autocorrelation Functions of Wavelets

$$\Phi(x) \stackrel{\Delta}{=} \int_{-\infty}^{+\infty} \varphi(y)\varphi(y-x)\,\mathrm{d}y$$

$$\Psi(x) \stackrel{\Delta}{=} \int_{-\infty}^{+\infty} \psi(y)\psi(y-x)\,\mathrm{d}y$$

- Symmetric and smoother than the corresponding $\varphi(x)$ and $\psi(x)$
- Convolution with $\Psi(x)$ essentially behaves as a differential operator $(\mathrm{d}/\mathrm{d}x)^L \Longleftarrow \hat{\Psi}(\xi) \sim O(\xi^L)$
- $\Phi(x)$ induces the symmetric iterative interpolation scheme

Autocorrelation Functions of Father Wavelets

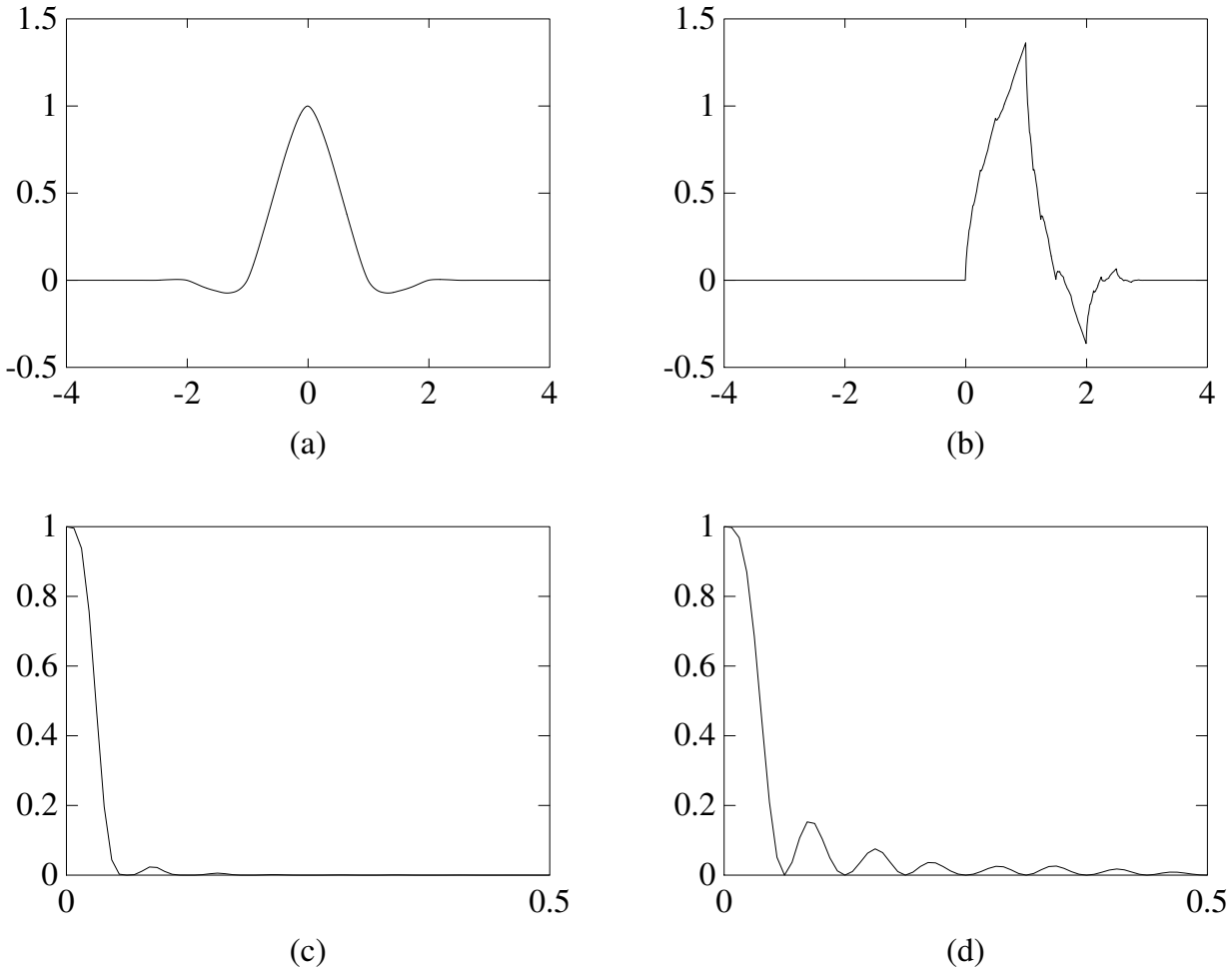

Figure: Φ vs φ in space and frequency domain.

Autocorrelation Functions of Mother Wavelets

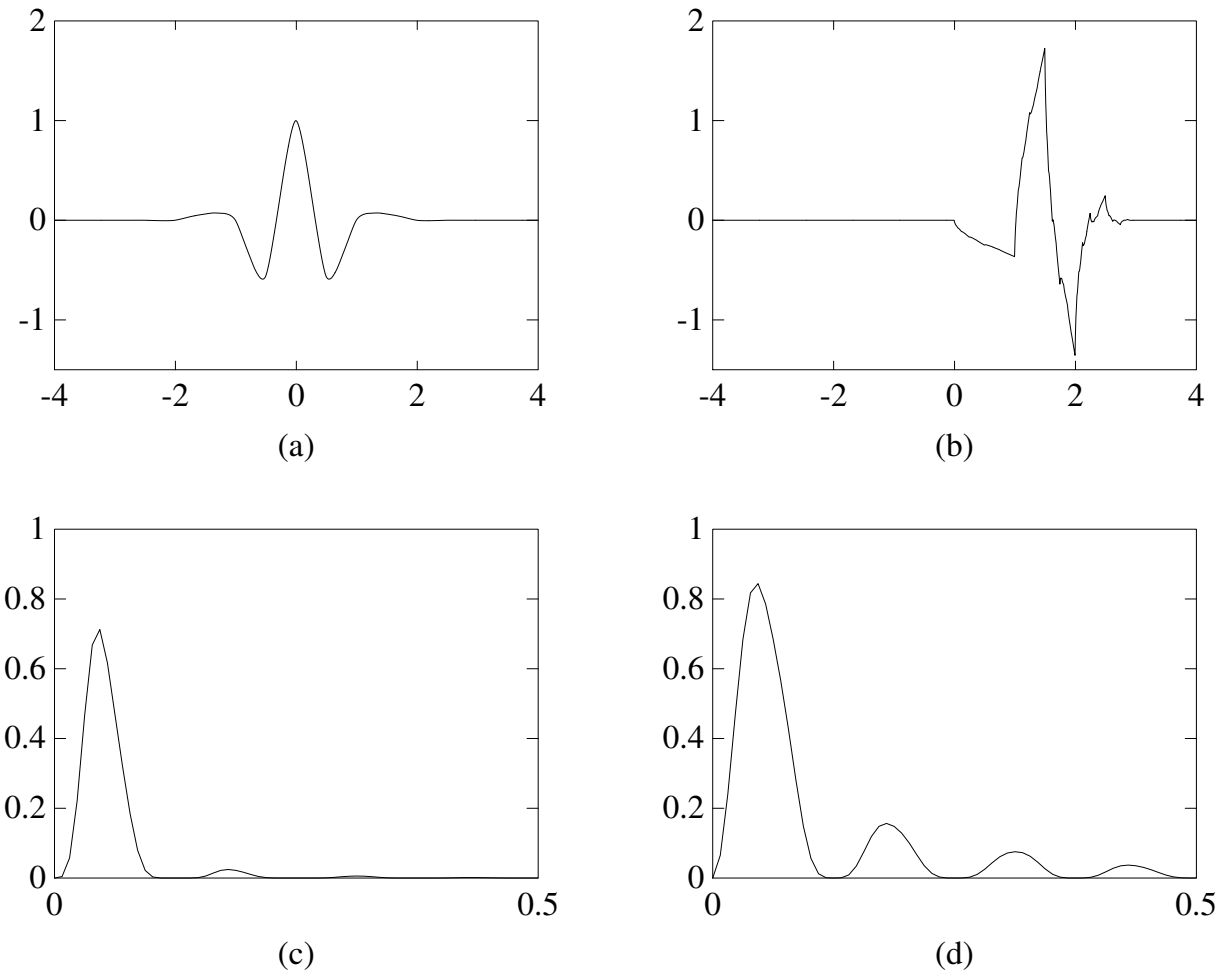

Figure: Ψ vs ψ in space and frequency domain.

Autocorrelation Functions of Wavelets . . .

- In Fourier domain:

$$\hat{\Phi}(\xi) = |\hat{\varphi}(\xi)|^2 \quad \text{and} \quad \hat{\Psi}(\xi) = |\hat{\psi}(\xi)|^2.$$

- Values at integer points:

$$\Phi(k) = \delta_{0k} \quad \text{and} \quad \Psi(k) = \delta_{0k}.$$

- Difference of two autocorrelation functions:

$$\hat{\Phi}(\xi) + \hat{\Psi}(\xi) = \hat{\Phi}(\xi/2),$$

or equivalently,

$$\Psi(x) = 2\Phi(2x) - \Phi(x).$$

Comparison with LoG and DOG functions

$$\Psi(x) = 2\Phi(2x) - \Phi(x).$$

vs

$$\begin{aligned} \frac{\mathrm{d}^2}{\mathrm{d}x^2} G(x;\sigma) &\approx G(x;a\sigma) - G(x;\sigma) \\ &= aG(ax;\sigma) - G(x;\sigma), \end{aligned}$$

where

$$G(x;\sigma) = \frac{1}{\sqrt{2\pi}\sigma} \mathrm{e}^{-x^2/2\sigma^2},$$

and $a = 1.6$ as Marr suggested.

Autocorrelation Functions of Wavelets . . .

- Two-scale difference equations:

$$\Phi(x) = \Phi(2x) + \frac{1}{2}\sum_{l=1}^{L/2} a_{2l-1}\left(\Phi(2x-2l+1) + \Phi(2x+2l-1)\right),$$

$$\Psi(x) = \Phi(2x) - \frac{1}{2}\sum_{l=1}^{L/2} a_{2l-1}\left(\Phi(2x-2l+1) + \Phi(2x+2l-1)\right),$$

where $\{a_k\}$ are the autocorrelation coefficients of the filter H,

$$a_k = 2\sum_{l=0}^{L-1-k} h_l h_{l+k} \quad \text{for} \quad k = 1, \ldots, L-1,$$

$$a_{2k} = 0 \quad \text{for} \quad k = 1, \ldots, L/2-1.$$

Autocorrelation Functions of Wavelets . . .

- Compact supports:

$$\text{supp } \Phi(x) = \text{supp } \Psi(x) = [-L+1, L-1].$$

- Vanishing moments:

$$\int_{-\infty}^{+\infty} x^m \Psi(x)\,\mathrm{d}x = 0, \qquad \text{for} \quad 0 \le m \le L-1,$$

$$\int_{-\infty}^{+\infty} x^m \Phi(x)\,\mathrm{d}x = 0, \qquad \text{for} \quad 1 \le m \le L-1,$$

$$\int_{-\infty}^{+\infty} \Phi(x)\,\mathrm{d}x = 1.$$

Outline

Autocorrelation Shell Representation

- A non-orthogonal shift-invariant representation using dilations and translations of $\Phi(x)$ and $\Psi(x)$
- Contains coefficients of all circular shifts of the original signal
- Convertible to the orthonormal shell representation on each scale separately
- Zero-crossings of the difference signals correspond to multiscale edges
- Computational cost is still $O(N \log_2 N)$

Autocorrelation Shell Representation . . .

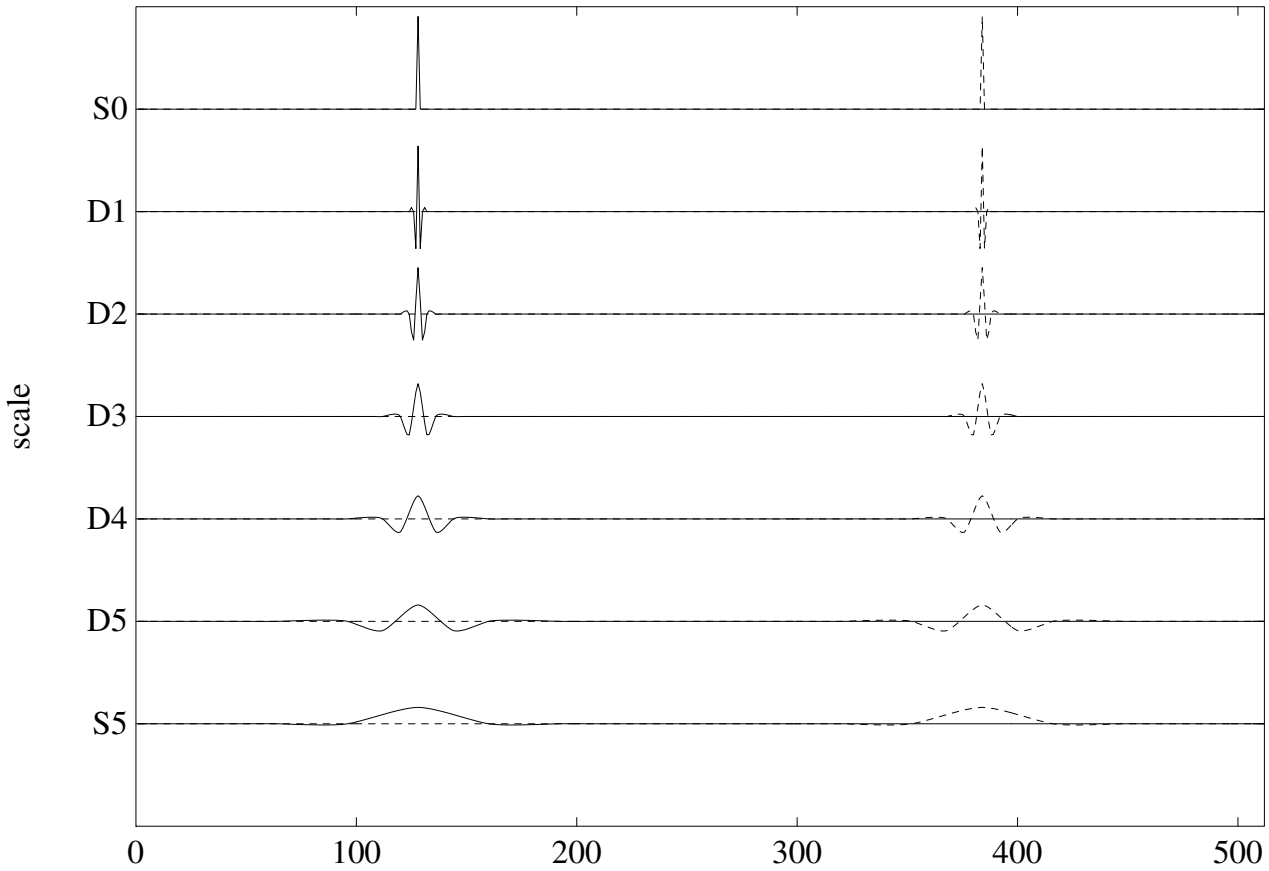

Figure: ACS representation of two spikes.

Autocorrelation Shell

- An autocorrelation shell is a set of functions

$$\{\Psi_{j,k}(x)\}_{1\le j\le J,\ 0\le k\le N-1} \quad \text{and} \quad \{\Phi_{J,k}(x)\}_{0\le k\le N-1},$$

where

$$\Phi_{j,k}(x) \stackrel{\Delta}{=} 2^{-j/2}\Phi(2^{-j}(x-k)), \Psi_{j,k}(x) \stackrel{\Delta}{=} 2^{-j/2}\Psi(2^{-j}(x-k))$$

- The autocorrelation shell coefficients of a function $f \in \mathcal{V}_0$, $f = \sum_{k=0}^{N-1} s_k^0 \varphi_{0,k}$, are $\{D_k^j\}_{1\le j\le J,\ 0\le k\le N-1}$ and $\{S_k^J\}_{0\le k\le N-1}$, where

$$S_k^j = \int f_s^j(x) 2^{-j/2} \widetilde{\varphi}_{j,k}(x)\,\mathrm{d}x, \quad D_k^j = \int f_d^j(x) 2^{-j/2} \widetilde{\psi}_{j,k}(x)\,\mathrm{d}x,$$

$$f_s^j(x) \stackrel{\Delta}{=} \sum_{\ell=0}^{N-1} s_\ell^j \varphi(x-\ell), \quad f_d^j(x) \stackrel{\Delta}{=} \sum_{\ell=0}^{N-1} d_\ell^j \varphi(x-\ell),$$

s_ℓ^j, d_ℓ^j are the orthonormal shell coefficients.

Autocorrelation Shell ...

An important relation between the original samples $\{s_k^0\}$ and the autocorrelation shell coefficients is:

Proposition

$$\sum_{k=0}^{N-1} S_k^j \Phi_{0,k} = \sum_{k=0}^{N-1} s_k^0 \Phi_{j,k}$$

$$\sum_{k=0}^{N-1} D_k^j \Phi_{0,k} = \sum_{k=0}^{N-1} s_k^0 \Psi_{j,k}.$$

Autocorrelation Shell Representation . . .

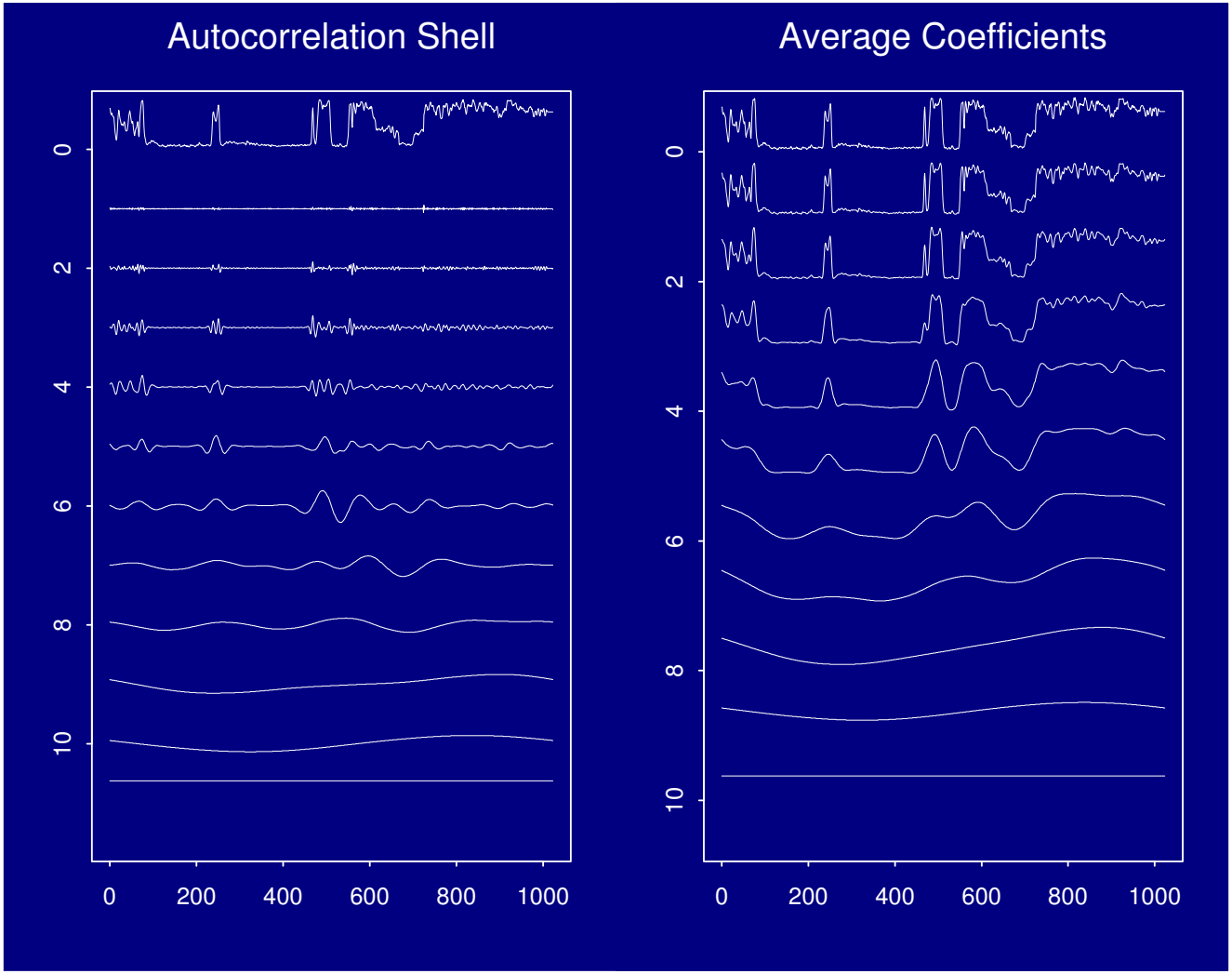

Figure: ACS representation of the real signal.

A Fast Decomposition Algorithm

Rewriting the two-scale difference equations:

$$\frac{1}{\sqrt{2}}\Phi(x/2) = \sum_{k=-L+1}^{L-1} p_k \Phi(x-k), \quad \frac{1}{\sqrt{2}}\Psi(x/2) = \sum_{k=-L+1}^{L-1} q_k \Phi(x-k),$$

where

$$p_k = \begin{cases} 2^{-1/2} & \text{for } k = 0, \\ 2^{-3/2} a_{|k|} & \text{for } k = \pm 1, \pm 3, \ldots, \pm(L-1), \\ 0 & \text{for } k = \pm 2, \pm 4, \ldots, \pm(L-2), \end{cases}$$

$$q_k = \begin{cases} 2^{-1/2} & \text{for } k = 0, \\ -p_k & \text{otherwise.} \end{cases}$$

A Fast Decomposition Algorithm

- We view these coefficients as filters $P = \{p_k\}_{-L+1 \le k \le L-1}$ and $Q = \{q_k\}_{-L+1 \le k \le L-1}$.
  - $p_k = p_{-k}$ and $q_k = q_{-k}$.
  - Only $L/2 + 1$ distinct non-zero coefficients.
- Using these filters P and Q, we compute

$$S_k^j = \sum_{l=-L+1}^{L-1} p_l S_{k+2^{j-1}l}^{j-1},$$

$$D_k^j = \sum_{l=-L+1}^{L-1} q_l S_{k+2^{j-1}l}^{j-1}.$$

Familiar Examples

- The Haar wavelet:

$$\{p_k\} = \frac{1}{\sqrt{2}}\left\{\frac{1}{2}, 1, \frac{1}{2}\right\}, \quad \{q_k\} = \frac{1}{\sqrt{2}}\left\{-\frac{1}{2}, 1, -\frac{1}{2}\right\}.$$

- The Daubechies wavelet with $L = 2M = 4$:

$$\{p_k\} = \frac{1}{\sqrt{2}}\left\{-\frac{1}{16}, 0, \frac{9}{16}, 1, \frac{9}{16}, 0, -\frac{1}{16}\right\},$$

$$\{q_k\} = \frac{1}{\sqrt{2}}\left\{\frac{1}{16}, 0, -\frac{9}{16}, 1, -\frac{9}{16}, 0, \frac{1}{16}\right\}.$$

- The Shannon wavelet: for $k \in \mathbb{Z}$,

$$p_k = \frac{1}{\sqrt{2}}\,\mathrm{sinc}(k/2),\ q_k = \frac{1}{\sqrt{2}}\left(2\,\mathrm{sinc}(k) - \mathrm{sinc}(k/2)\right).$$

A Fast Reconstruction Algorithm

- Using $\hat{\Phi}(\xi) + \hat{\Psi}(\xi) = \hat{\Phi}(\xi/2)$, we obtain a simple reconstruction formula,

$$S_k^{j-1} = \frac{1}{\sqrt{2}} \left(S_k^j + D_k^j \right),$$

for $j = 1, \ldots, J, \;\; k = 0, \ldots, N-1$

- Given the autocorrelation shell coefficients $\{D_k^j\}_{1 \le j \le J, \; 0 \le k \le N-1}$ and $\{S_k^J\}_{0 \le k \le N-1}$,

$$s_k^0 = 2^{-J/2} S_k^J + \sum_{j=1}^{J} 2^{-j/2} D_k^j,$$

for $k = 0, \ldots, N-1$.

Outline

An Iterative Interpolation Scheme

- $\Phi(x)$ induces the symmetric iterative interpolation scheme of S.Dubuc.
- This interpolation scheme fills the gap between the following two extreme cases:
- The Haar father wavelet $\longrightarrow$ linear interpolation

$$\Phi_{\text{Haar}}(x) = \begin{cases} 1+x & \text{for } -1 \le x \le 0, \\ 1-x & \text{for } 0 \le x \le 1, \\ 0 & \text{otherwise.} \end{cases}$$

- The Shannon father wavelet $\longrightarrow$ band-limited interpolation

$$\Phi_\infty(x) = \varphi_\infty(x) = \text{sinc}(x).$$

An Iterative Interpolation Scheme . . .

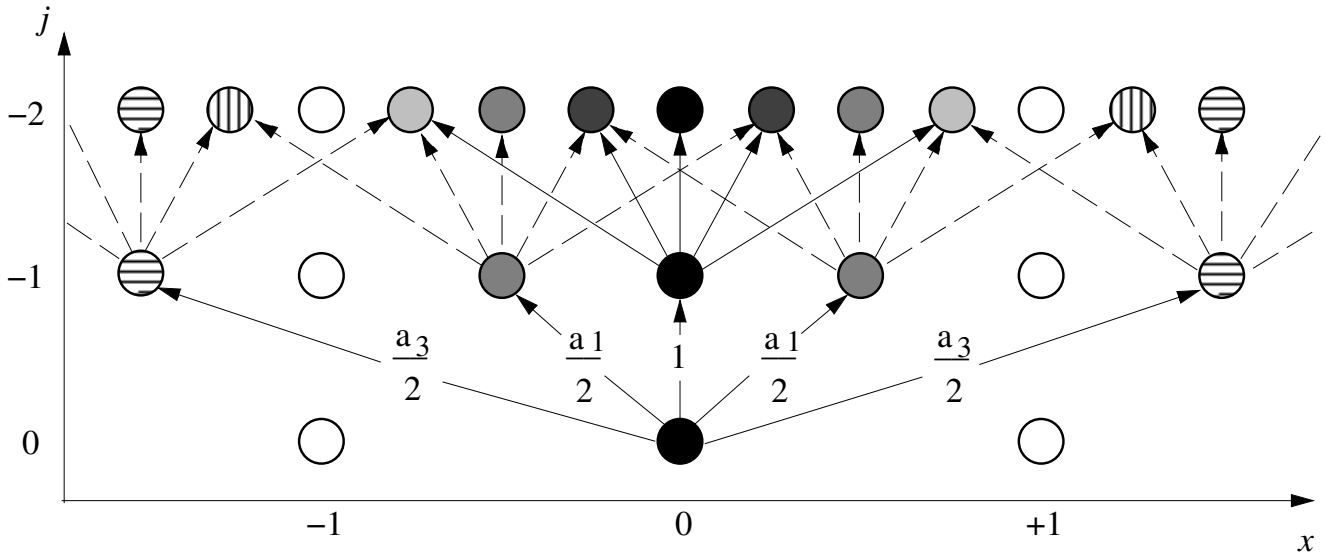

Figure: Dubuc iterative interpolation with $L = 4$.

Edge Detection via Iterative Interpolation Scheme . . .

- Essentially, Dubuc's iterative interpolation scheme upsamples the discrete data, i.e. goes up from coarser to finer scales by filling new points smoothly between the sample points without changing the original sample values.
- As a result, we can evaluate $\Phi(x)$, $\Phi'(x)$, $\Psi(x)$, and $\Psi'(x)$ at any given point $x \in \mathbb{R}$ within the prescribed numerical accuracy.
- Can iteratively zoom in the interval until it reaches $[x - \epsilon, x + \epsilon]$. The derivative is merely a convolution of the values of Φ in that interval with some discrete filter coefficients.

Outline

Reconstruction of Signals from Zero-Crossings

- Marr's conjecture
- Previous attempts
  - Curtis & Oppenheim ('87): Multiple level crossings, Fourier coefficients, no multiscale
  - Hummel & Moniot ('89): Scale-space, heat equation, stability problem, empirical use of slope information
  - Mallat ('91): Dyadic wavelet transform, wavelet maxima, POCS (projection onto convex sets) for reconstruction
- Can we reconstruct the original signal from zero-crossings (and slopes at these zero-crossings, if necessary) of the autocorrelation shell representation of that signal?

Advantages using ACS

- Zero-crossings of the ACS representation are related to multiscale edges of the original signal.
- We have an efficient iterative algorithm to pinpoint these zero-crossings (via the Dubuc's iterative interpolation).
- Proposition allows us to set up a system of linear algebraic equations to reconstruct the original signal.
- Can explicitly show that the slope information at each zero-crossing is necessary.

Proposed Method (See Saito & Beylkin '93 for the details)

1. Compute zero-crossing locations and slopes at these locations in the ACS representation using the symmetric iterative interpolation scheme.
2. Set up a system of linear algebraic equations (often sparse), where the unknown vector is the original signal itself and the entries of the matrix are computed from the values of $\Phi(x), \Phi'(x)$ at the integer translates of the zero-crossing locations.
3. Solve the linear system to find the original signal.

Note that one can introduce heuristic constraints such as the distance between the adjacent zero-crossings at the jth scale does not exceed $2^{j+1}(L-1)$, which may stabilize the linear system solver.

1D Examples

- The 1D profile of the image of the size 512.
  In this case, the size of the matrix $\mathbf{A}$ is 1852 by 512. The relative L^2 error of the reconstructed signal compared with the original signal is 5.674436×10^{-13}. The accuracy threshold ϵ was set to 10^{-14}. In this example, the constraints did not make any difference since the zero-crossings are "dense".
- A unit impulse $\{\delta_{31,k}\}_{k=0}^{63}$.
  In this case, the size of the matrix $\mathbf{A}$ is 56×64. This example needs constraints. The relative L^2 error with the constraints is 7.417360×10^{-15} whereas the error of the solution by the generalized inverse without the constraints is 3.247662×10^{-4}.

Outline

Conclusions

- The autocorrelation wavelets behave like edge detectors with various scales
- Can characterize the type of edges (singularities) from the decay of the ACS coefficients across scales
- The autocorrelation wavelets are symmetric, sufficiently smooth, and induce a symmetric iterative interpolation scheme
- The autocorrelation shell is a shift-invariant representation containing the coefficients of all circulant shifts of the original signal with the cost $O(N \log_2 N)$
- The original signal is also reconstructed by solving a system of linear algebraic equations derived from the zero-crossings (and slopes)

Outline

References

- V. Bruce, P. R. Green, & M. A. Georgeson, *Visual Perception*, 4th Ed., Psychology Press, 2003.
- I. Daubechies, *Ten Lectures on Wavelets*, SIAM, 1992.
- R. L. De Valois & K. K. De Valois, *Spatial Vision*, Oxford Univ. Press, 1988.
- D. H. Hubel, *Eye, Brain, and Vision*, Scientific American Library, 1995.
- S. Jaffard and Y. Meyer and R. D. Ryan, *Wavelets: Tools for Science & Technology*, SIAM, 2001.
- S. Mallat, "Zero-crossings of a wavelet transform," *IEEE Trans. Info. Theory*, vol. 37, pp.1019–1033, 1991.
- D. Marr, *Vision*, W. H. Freeman and Co., 1982.
- N. Saito & G. Beylkin, "Multiresolution representations using the auto-correlation functions of compactly supported wavelets," *IEEE Trans. Sig. Proc.*, vol. 41, pp.3584–3590, 1993.
- B. A. Wandell, *Foundations of Vision*, Sinauer Associates, Inc., 1995.